A Generalized Load-Transfer Modeling Framework for Tensioned Anchors Integrating Adhesion–Friction-Based Interface Model

Changfu Chen, Ph.D.[1]; Shimin Zhu[2]; Genbao Zhang, Ph.D.[3]; Amr M. Morsy, Ph.D.[4]; Jorge G. Zornberg, Ph.D., P.E. F.ASCE[5]; and Fengshan Mao[6]

Abstract: The load-transfer mechanism of tensioned anchors is primarily concerned with in-service performance, which depends on the bond–slip behavior of anchoring interface. Because the interface bond–slip behavior is conventionally modeled using epistemic experience of specific researchers and/or back analysis of specific in situ testing results, it is challenging to develop a straightforward load-transfer analysis with extensive applicability. A generalized load-transfer modeling framework was implemented in this work by incorporating a versatile interface bond–slip model that can be derived from experimental characterization of respective types of element-anchoring interface. The adhesion and friction were modeled with interface slip to constitute the interface bond using rational and exponential functions, respectively. The pullout tests on element-scale and large-scale specimens of a typical anchor type (i.e., tensioned steel tube embedded in cemented soils) were carried out to calibrate the parameters of the interface model and to validate the predicting capability of the modeling framework, respectively. In addition, the versatility of this load-transfer modeling framework was examined for two other anchor types reported in the literature (i.e., tensioned rock anchor and tensioned GFRP anchor embedded in sands). The consistent good agreements between predictions and measurements of these anchor types verified the effectiveness and applicability of the generalized load-transfer modeling framework. Based on the load-transfer analysis for the tensioned steel tube in model testing, a parametric study was performed to investigate the impact of axial stiffness and bond length on load-transfer responses of the tensioned anchor. **DOI: 10.1061/(ASCE)GM.1943-5622.0002338**.

Author keywords: Interface bond–slip model; Load-transfer modeling framework; Element anchoring interface; Pullout response; Tensioned anchors.

Introduction

Anchorage technology was originally used in mining engineering and has been extensively applied to geomaterial retention, such as in slopes, retaining walls, tunnels, deep excavations, and other solutions in civil engineering (Farmer 1975; Li and Stillborg 1999; Kılıc et al. 2002; Chu and Yin 2005; Yin and Zhou 2009; Zhu et al. 2021). The loading mechanisms that take place in anchorage systems involve transfer of axial loads sustained by the anchor to the surrounding stable geomaterial mass through interface shear resistance within constrained geomaterial deformations (Li and Stillborg 1999; Kılıc et al. 2002). Generally, a tensioned grouted anchor is comprised of an anchor head, a tension rod, and grout. Failure modes associated with such anchors include rupture of the tension rod, debonding of the tension rod and the grout, and debonding of the grout and the surrounding geomaterial. The rod tension capacity can primarily be controlled by tensile properties of the rod. However, controlling the interface bond capacity can be quite challenging due to the complexity of the load-transfer mechanisms, which can be sensitive to several influence factors, including the structural form of the anchor, geomaterial and grout properties, and interface behavior among tension rod, grout, and geomaterial (Kılıc et al. 2002; Chu and Yin 2005).

Current design guidelines and codes of tensioned anchor assume idealized uniform distribution of interface bond stress over the entire bond length in determining the pullout resistance that simplifies the effects of the complex load-transfer mechanisms and geomaterial properties on the interface shear stress distribution (CECS 2005; GB 2013; CEN 2013; PTI 2014). This idealized stress distribution differs from that developed in the field. Several in situ and lab model tests were carried out to investigate the loading mechanism and improve the current design theory for anchors/soil nails (Farmer 1975; Kılıc et al. 2002; Rong et al. 2004; Chu and Yin 2005; Yin and Zhou 2009; Zhang et al. 2015). Different interface bond stress distributions over bond length between anchor and geomaterial were assumed to conduct theoretical load analysis of an anchor, typically exemplified by exponential distribution (Farmer 1975; Li and Stillborg 1999), neutral point distribution (Wang 1983; Hyett et al. 1996), and Mindlin

[1]Professor, College of Civil Engineering, Hunan Univ., Changsha, Hunan Province 410082, China. Email: cfchen@hnu.edu.cn

[2]Ph.D. Student, College of Civil Engineering, Hunan Univ., Changsha, Hunan Province 410082, China. ORCID: https://orcid.org/0000-0002-7464-8227. Email: smzhu@hnu.edu.cn

[3]Assistant Professor, College of Civil Engineering, Hunan City Univ., Yiyang, Hunan Province 413000, China (corresponding author). ORCID: https://orcid.org/0000-0001-8303-1010. Email: genbao@hncu.edu.cn

[4]Research Associate, School of Architecture, Building and Civil Engineering, Loughborough Univ., Leicestershire LE11 3TU, UK. Email: a.morsy@lboro.ac.uk

[5]Professor, Dept. of Civil, Architectural, and Environmental Engineering, Univ. of Texas, Austin, TX 78712. ORCID: https://orcid.org/0000-0002-6307-1047. Email: zornberg@mail.utexas.edu

[6]Ph.D. Student, College of Civil Engineering, Hunan Univ., Changsha, Hunan Province 410082, China. Email: mfengshan@hnu.edu.cn

Note. This manuscript was submitted on April 9, 2021; approved on December 6, 2021; published online on February 25, 2022. Discussion period open until July 25, 2022; separate discussions must be submitted for individual papers. This paper is part of the ***International Journal of Geomechanics***, © ASCE, ISSN 1532-3641.

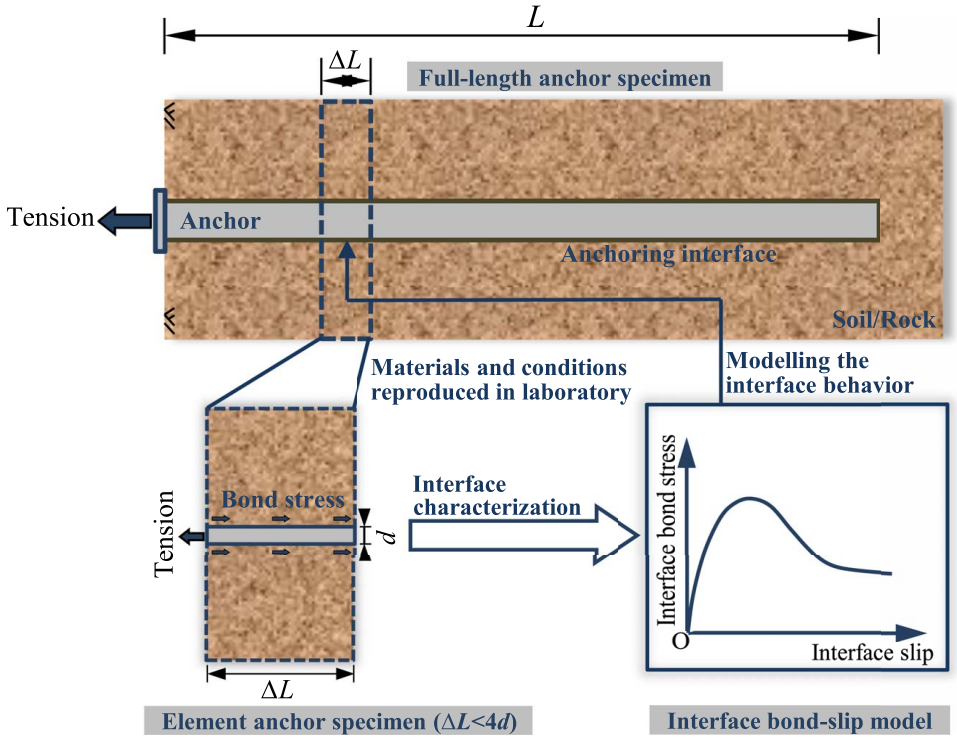

Fig. 1. Schematic of interface characterization using element anchor specimens (Method B).

solution-based distribution (You 2000). However, experimental investigations reported that the interface bond stress varies over the bond length, as interface shear resistance is progressively mobilized from the loaded end to the free end of the bond length (Farmer 1975; Rong et al. 2004). The aforementioned interface bond stress distribution assumptions were found to render unsatisfactory performance in characterizing the variation of bond stress with increasing tension for anchors in the field; consequently, the force analysis of an anchor based on the load-transfer method has been adopted in several research studies (Ren et al. 2010; Martín et al. 2011; Hong et al. 2012; Ma et al. 2013, 2016; Huang et al. 2014; Zhang et al. 2015; Zou and Zhang 2019).

The load-transfer analysis requires proper characterization of interface bond–slip behavior, which can be implemented using an interface bond–slip model. The interface bond–slip model and its parameters used in the current theoretical load-transfer modeling frameworks for anchors/soil nails were generally determined based on the epistemic experience of specific researchers and/or back analysis for the in situ test data, especially load-displacement data (Ren et al. 2010; Ma et al. 2013; Zou and Zhang 2019). It essentially used the tested mechanical boundary conditions at the anchor head for this method. This parameter calibration method is semiempirical, indirect, and restrained by the in situ test results and was called Method A in this paper. In fact, the mechanical behavior of the whole tensioned anchors/soil nails can be regarded as the integration of differential elements (Chen et al. 2015), as illustrated in Fig. 1. In addition, Benmokrane et al. (1995) pointed out that anchors with short bond length, of less than four times of the anchor diameter, could be employed to define the interface constitutive relationship. This is due to a uniform distribution of the interface shear stress over the short bond length (Martín et al. 2011; Ma et al. 2013; Zhang et al. 2020). It provided possibilities for calibrating the parameters of the interface bond–slip model using laboratory pullout test on element-scale anchoring specimens, which can be categorized as Method B. In contrast to Method A, Method B was recognized as a straightforward, robust, and generalizable method to derive interface model parameters.

This paper presents an integrated interface bond–slip model developed by modeling interface adhesion and friction resistance with a rational and an exponential function, respectively. A new load-transfer modeling framework of tensioned anchor was introduced based on the developed integrated interface bond–slip model. The measured pullout responses of model tests were compared with that predicted using the developed load-transfer modeling framework. Finally, a parametric study was conducted on the influence of the anchor axial stiffness and bond length on the ultimate pullout resistance. The remaining pullout responses of the tensioned anchor including the axial force and interface bond stress distributions were also investigated.

Review of Interface Bond–Slip Models

A bond–slip model is used to characterize the relationship between bond stress (i.e., interface shear stress) and slip displacement at the interface between two materials in contact, and it is sometimes referred to as interface shear stress–displacement (Ma et al. 2013; Chen et al. 2015). Numerous bond–slip models have been developed for interfaces of different materials, such as pile–soil interface, anchor–soil interface, and rebar–concrete interface, among others. In geotechnical engineering, the bond–slip model was first applied to the load-transfer analysis of a shaft pile and was called the pile load-transfer model (Kezdi 1957). Due to the similar geometry and loading mechanisms with shaft piles, the bond–slip model has been increasingly used in load-transfer analysis of anchors (Ren et al. 2010; Martín et al. 2011; Ma et al. 2013, 2016; Huang et al. 2014; Zhang et al. 2015; Zou and Zhang 2019).

Bond–slip models were introduced in several mathematical forms, including the exponential model (Kezdi 1957), the linear elastoplastic model (Satoru 1965), the hyperbolic model (Richard and Abbott 1975), and the parabolic model (Vijayvergiya 1977).

Int. J. Geomech., 2022, 22(5): 04022036

Recently, some researchers made improvements on available bond–slip models and developed new models to accommodate interfaces involving new applications of geomaterials and structures, such as the dual exponential model (Ma et al. 2013) and the rational-function model (Chen et al. 2015). Table 1 summarizes some of the common bond–slip models developed in interface characterization of anchors (or piles) embedded in various geomaterials.

These interface bond–slip models can be categorized into broken-line set and curved-line set according to their shapes. The broken-line bond-slip models are less friendly in application to load-transfer analysis of anchors as they require piecewise input of bond stress. For example, three-phase analysis needed for a bilinear model (Hong et al. 2012; Zhang et al. 2015), and five-phase analysis needed for a trilinear model (Ren et al. 2010). Conversely, the curved-line bond–slip models are merely appropriate to specific work conditions. For example, the hyperbolic model (Wong and Teh 1995) is suitable only for the special case of strain hardening; the exponential model (Yu and Liu 2005) and the dual exponential model (Ma et al. 2013; Huang et al. 2014) are suitable only for the special case of complete strain softening. Hence, a more generalized bond–slip model suitable for load-transfer analysis is still required to alleviate those defects of the previous models.

Table 1. Summary of common bond-slip models of geomaterial-structure interfaces

Reference	Expressions	Notations
Kezdi (1957)	$\tau = K\gamma z \tan\varphi[1-\exp(-ks/(s_f-s))]$	τ, s – interface bond stress and slip; K – lateral earth pressure coefficient; k – model parameter; γ, φ – soil unit weight and internal friction angle; s_f – peak shear displacement; z – depth.
Satoru (1965)	$\tau = \begin{cases} C_s s, & s \le s_f \\ \lvert\tau_r, & s > s_f \end{cases}$	C_s – coefficient; τ_r – residual shear strength.
Richard and Abbott (1975)	$\tau = \dfrac{E_s s}{[1+(E_s s/\tau_f)^n]^{1/n}}$	E_s – Young's modulus of soil; n – geometric coefficient of curve; τ_f – interface shear strength.
Vijayvergiya (1977)	$\tau = \tau_f(2\sqrt{s/s_f} - s/s_f)$	—
Kraft et al. (1981)	$\tau = \dfrac{G_0 s}{r_0 \cdot \ln[r_m/r_0 - \psi/1-\psi]}$	$\Psi = \tau R_f/\tau_f$; G_0 – initial shear modulus of soil; r_0, r_m – radius of pile and influence radius of settlement; R_f – fitting parameter.
Heydinger and O'Neill (1986)	$\tau = \dfrac{E_{\tau s}(s/d)}{[1+(E_{\tau s}(s/d)/\tau_f)^m]^{1/m}}$	$E_{\tau s}$ – initial slope of $\tau - s/d$ curve; m – geometric coefficient of curve; d – diameter of pile.
Cao (1986)	$\tau = \begin{cases} \lvert k_e s, & 0 \le s \le s_f \\ \lvert k_e s_f + k_p(s-s_r), & s_f < s \le s_r \\ \lvert\tau_r, & s > s_r \end{cases}$	k_e – stiffness of elastic phase; k_p – stiffness of plastic phase; s_r – displacement corresponding to τ_r.
Chen et al. (1994)	$\tau = \begin{cases} \lvert k_e s, & 0 \le s \le s_f \\ \lvert k_e s_f + k_p(s-s_r), & s > s_f \end{cases}$	k_e – stiffness of elastic phase. k_p – stiffness of plastic phase
Wong and Teh (1995)	$\tau = \dfrac{s}{(1/k_s) + R_f(s/\tau_f)}$	R_f – failure ratio; k_s, τ_f – initial shear stiffness and shear strength of interface.
Zhu and Chang (2002)	$s = \dfrac{\tau r_0}{G_s g}\ln\left[\dfrac{(r_m/r_0)^g - f(\tau/\tau_f)^g}{1-f(\tau/\tau_f)^g}\right]$	r_0, r_m – radius of pile and influence radius; G_s – shear modulus; f, g – undetermined parameters.
Cai et al. (2004)	$\tau = \begin{cases} ks, & s \le s_f \\ \tau_r, & s > s_f \end{cases}$	k – shear stiffness; s_f – peak shear displacement.
You (2004)	$\tau = \begin{cases} k_1 s, & 0 \le s \le s_1 \\ k_1 s_1 + k_2(s-s_1), & s_1 < s \le s_2 \\ \tau_3, & s > s_2 \end{cases}$	k_1, k_2 – stiffness coefficients of skin friction; s_1 – elastic displacement limit; s_2 – plastic displacement limit; τ_3 – residual shear strength.
Yu and Liu (2005)	$\tau = ase^{-bs}$	a, b – undetermined parameters.
Zhang and Zhang (2012)	$\tau = s(a+cs)/(a+bs)^2$	a, b, c – undetermined parameters.
Ma et al. (2013)	$\tau = \dfrac{Ed}{4}\dfrac{a}{b^2}e^{-s/a}(1-e^{-s/a})$	a, b – undetermined parameters.
Chen et al. (2015)	$\tau = \tau_f \dfrac{Us_f s + (V-1)s^2}{s_f^2 + (U-2)s_f s + Vs^2}$	U, V – undetermined parameters.
Zhu et al. (2021)	$\tau = \exp[-(s/\xi)^\eta] \cdot \frac{s}{s_{cr}+s}(\sigma_n \tan\varphi_i + c_i) + \{1-\exp[-(s/\xi)^\eta]\} \cdot (\sigma_n \tan\varphi_c + c_c)$	σ_n – interface normal stress; ξ, η – probability parameters; s_{cr}, φ_i, c_i, φ_c, c_c, – undetermined model parameters.

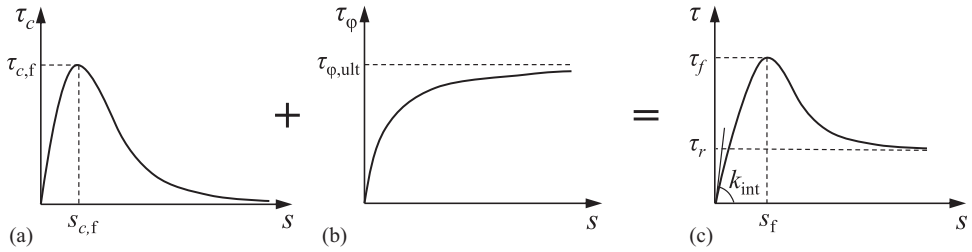

Fig. 2. Schematic of anchor-geomaterial interface bond–slip model: (a) interface adhesion versus interface slip; (b) interface friction versus interface slip; and (c) interface bond stress versus interface slip.

Adhesion-Cohesion-Based Interface Bond–Slip Model

Model Development

Generally, anchor–geomaterial interface bond strength consists of interface adhesion τ_c and interface friction τ_φ (Chu and Yin 2005; Yin and Zhou 2009), as depicted in Fig. 2. Some researchers consider the contribution of mechanical interlocking to interface bond strength for anchors with very rough interface surface and/or with ribs on the interface (Li and Stillborg 1999; ACI 2003). To facilitate modeling, the interlocking contribution was assumed as the composition of interface adhesion.

Interface adhesion is comprised of electrostatic attraction, van der Waals forces, and interparticle chemical cohesion. Interface adhesion is increasingly mobilized with increasing slip displacement to a certain slip magnitude that corresponds to the peak adhesion, beyond which the interface adhesion decreases rapidly with increasing slip displacement and vanishes completely due to the decoupled contact over the interface (ACI 2003). Accordingly, the relationship between interface adhesion τ_c and interface slip s was modeled as shown in Fig. 2(a).

Interface friction is mobilized with the slip displacement over the surface of the contacting material, and depends on the normal pressure and surface roughness (Chu and Yin 2005). Interface shear resistance for reinforcements [e.g., steel section (Martinez et al. 2015; Kishida and Uesugi 1987), geosynthetics (Zhang et al. 2015; Liu et al. 2009), concrete (Toufigh et al. 2017)] embedded in cohesionless geomaterials such as sands and gravels is mainly attributed to the interface friction. Experimental findings from direct shear and torsional shear tests suggest that interfaces exhibit strain-hardening behavior when loose soils or smooth interfaces are involved (Kishida and Uesugi 1987; Liu et al. 2009; Toufigh et al. 2017; Hu and Pu 2004; Moayed et al. 2019), whereas interfaces exhibit strain-softening behavior when dense soils or rough interfaces are involved (Kishida and Uesugi 1987; Hu and Pu 2004; Toufigh et al. 2017; Moayed et al. 2019). For both interface strain-softening and interface strain-hardening behaviors, interface friction is mobilized with increasing interface slip displacements. Accordingly, the interface friction τ_φ was modeled to mobilize with increasing interface slip s to a certain limit, which corresponds to the ultimate interface friction resistance $\tau_{\varphi,ult}$, as depicted in Fig. 2(b). Note that both interface adhesion and interface friction exist together for interface strain softening because the interlocking contribution is included in interface adhesion, especially for dense soils.

In general, interface adhesion develops simultaneously with interface friction with increasing interface slip, as shown in Fig. 2(c). Interface bond stress increases within a range of interface slip at which both interface adhesion and interface friction components are mobilized. Following the peak (maximum mobilization) of the adhesion component, the bond strength may continue to increase if the friction mobilization increment is greater than that of the adhesion decrement. Then, the bond strength decreases when the cohesion decrement is greater than that of the friction increment. Finally, when the cohesion vanishes at a large slip magnitude, bond stress retains the contribution of the interface friction only, which corresponds to the residual bond strength τ_r (i.e., friction limit $\tau_{\varphi,ult}$). The evolution of interface bond strength with increasing interface slip was verified by the measurements in reported anchor pullout tests (Kishida and Uesugi 1987; Yin and Zhou 2009; Chen et al. 2015; Toufigh et al. 2017; Zhu et al. 2021).

Based on the observations of the bond strength characteristic curves, the development of interface adhesion and interface friction over increasing interface slip [shown in Figs. 2(a and b), respectively] were modeled by a rational function and an exponential function presented in Eqs. (1*a*) and (1*b*), respectively, as

$$\tau_c(s) = \frac{abs}{1 + (bs)^n} \tag{1a}$$

$$\tau_\varphi(s) = c(1 - e^{-ds}) \tag{1b}$$

By integrating the interface adhesion and interface friction, the anchor–geomaterial interface bond–slip model can be expressed as

$$\tau(s) = \tau_\varphi(s) + \tau_c(s) = \frac{abs}{1 + (bs)^n} + c(1 - e^{-ds}) \tag{2}$$

where $\tau =$ interface bond stress; $s =$ interface slip displacement; and n, a, b, c, and $d =$ bond–slip model parameters. Specifically, a is governed by the magnitude of adhesion τ_c; b is governed by the magnitude of slip displacement $s_{c,f}$ corresponding to the peak adhesion $\tau_{c,f}$, and the geometry for the adhesion curve; c is governed by the magnitude of interface friction τ_φ; d is governed by the curvature of the interface friction curve; and n is governed by the adhesion. The value of n can be determined based on the shape of the bond–slip curve where a steeper slope of post-peak bond stress reduction corresponds to a greater value of n. Generally, the value of $n = 4$ can be appropriate for most anchor cases (e.g., three case examples presented in this work).

It should be noted that interface adhesion and interface friction are not mobilized simultaneously for all cases in practice; special cases may exist where bond strength constitutes of adhesion only or interface friction only. These special cases can be summarized as follows:

Special Case A: Interface bond strength consists of adhesion only due to the absence of interface friction or negligible interface friction. This case exists for anchors embedded in cohesive geomaterials with insignificant internal friction angles, such as anchors embedded in resin (Ma et al. 2013). In this case, the interface bond–slip model can be rewritten as

$$\tau(s) = \tau_c(s) = \frac{abs}{1 + (bs)^n} \tag{3}$$

Special Case B: Interface bond strength consists of interface friction only due to the absence of interface adhesion or negligible adhesion. This case exists for anchors embedded in geomaterials that are cohesionless or with insignificant cohesion, such as anchors embedded in loose sands and gravels. In this case, the interface bond–slip model can be rewritten as

$$\tau(s) = \tau_{\varphi}(s) = c(1 - e^{-ds}) \tag{4}$$

Determination of Model Parameters

It is reasonable to use information of characteristic points (referred to as interface characteristic parameters) in the bond–slip curve in determining the value of the four model parameters (a, b, c, and d). These points include the peak bond stress τ_f, the slip displacement corresponding to peak bond stress s_f, the residual bond stress τ_r, and the initial shear stiffness k_{ini}, as shown in Fig. 2(c). The procedures of determining interface characteristic parameters as well as model parameters are described next in detail.

Determination of Interface Characteristic Parameters

Currently, the interface characteristic parameters were generally determined based on the epistemic experience of specific researchers and/or back analysis for the in situ test data (Ren et al. 2010; Ma et al. 2013; Huang et al. 2014; Zou and Zhang 2019), called Method A in this paper. For example, Ren et al. (2010) performed analysis on the characteristic points of the measured load-displacement curve; Ma et al. (2013) performed regression analysis on the measured load-displacement curve. Method A has been extensively used in designing anchorage systems. This approach is semiempirical and indirect, and its reliability depends on the accuracy of the derived interface characteristic parameters and the experience of designers.

Benmokrane et al. (1995) reported that pullout tests on element anchors with encapsulating lengths less than four times the anchor diameter are reliable to use in characterizing anchor–geomaterial interface behavior. This is because interface bond stress is fairly uniformly distributed over such short bond lengths (Martín et al. 2011; Ma et al. 2013; Chen et al. 2018). Inspired by this, to alleviate the aforementioned problems of Method A, a new method that determines the interface characteristic parameters using laboratory pullout test on element anchors was proposed in this paper, which is named Method B. Although the effectiveness of this approach relies highly on the modeling consistency of material properties and boundary conditions in element tests with those of the anchors in field, the interface characteristic parameters derived using this approach are recognized as more accurate and reliable than those of Method A. The use of Method B is demonstrated next.

Determination of Interface Bond–Slip Model Parameters

In general, considering the presence of both interface adhesion and interface friction, the following conditions can be assumed in solving model parameters:

Condition A: interface slip s_f corresponds to peak interface bond stress τ_f:

$$\tau(s_f) = \frac{abs_f}{1 + (bs_f)^4} + c(1 - e^{-ds_f}) = \tau_f \tag{5}$$

Condition B: the derivative of bond stress over slip corresponding to interface slip s_f is zero:

$$\left.\frac{d\tau}{ds}\right|_{(s=s_f)} = \frac{ab(1 - 3b^4 s_f^4)}{(1 + b^4 s_f^4)^2} + cde^{-ds_f} = 0 \tag{6}$$

Condition C: interface bond stress approaches the residual bond stress τ_r when the slip s develops infinitely:

$$\lim_{s\to\infty} \tau(s) = \lim_{s\to\infty} \frac{abs}{1 + (bs)^4} + c(1 - e^{-ds}) = \tau_r \tag{7}$$

Condition D: initial shear stiffness corresponds to the derivative of bond stress over slip at the origin of bond–slip curve:

$$\left.\frac{d\tau}{ds}\right|_{(s=0)} = ab + cd = k_{\text{ini}} \tag{8}$$

By combining of Eqs. (5)–(8), the bond–slip model parameters can be expressed as

$$a = \frac{k_{\text{ini}} - k\tau_f D}{b} \tag{9a}$$

$$b = \frac{1}{s_f}\sqrt[4]{\frac{(k_{\text{ini}} - k\tau_f D)s_f}{\tau_f + k\tau_f(e^{-Ds_f} - 1)} - 1} \tag{9b}$$

$$c = \tau_r = k\tau_f \tag{9c}$$

$$d = \frac{(k\tau_f + k_{\text{ini}}B - \tau_f - k\tau_f A) - \sqrt{(k\tau_f + k_{\text{ini}}B - \tau_f - k\tau_f A)^2 + 4kk_{\text{ini}}\tau_f AB}}{2k\tau_f B} \tag{9d}$$

where bond stress ratio k = ratio of peak bond stress to residual bond stress,

$$k = \frac{\tau_f}{\tau_r} \tag{10a}$$

and

$$A = \frac{1 - 3b^4 s_f^4}{(1 + b^4 s_f^4)^2} \tag{10b}$$

$$B = \frac{s_f}{1 + b^4 s_f^4} \tag{10c}$$

$$D = \frac{(k\tau_f + k_{\text{ini}}B - \tau_f - k\tau_f A) - \sqrt{(k\tau_f + k_{\text{ini}}B - \tau_f - k\tau_f A)^2 + 4kk_{\text{ini}}\tau_f AB}}{2k\tau_f B} \tag{10d}$$

Note that the value of b can be solved using iteration with Eq. (9b), and substitution of b into Eqs. (9a) and (9d) can solve the values of a and d. For special cases with the absence of interface adhesion or interface friction, model parameters were also derived accordingly.

For Special Case A (adhesion only), two model parameters a and b in Eq. (3) can be determined in terms of three interface characteristic parameters τ_f, and s_f using Conditions A and B as

$$a = \frac{4\sqrt[4]{3}}{3}\tau_f \tag{11a}$$

$$b = \frac{1}{\sqrt[4]{3}s_f} \tag{11b}$$

For Special Case B (friction only), two model parameters c and d in Eq. (4) can be determined in terms of two interface characteristic parameters τ_r and k_{int} using Conditions C and D as

$$c = \tau_r = k\tau_f \tag{12a}$$

$$d = \frac{k_{\text{ini}}}{k\tau_f} \tag{12b}$$

where the value of bond stress ratio $k = 1$.

Use of Method B Exemplified in Element Pullout Tests of Steel Tube Embedded in Cemented Soils

The element-scale specimen of steel tube embedded in cemented soils was prepared using a specially designed pullout test setup, with details described by Chen et al. (2018, 2020). The specimen was comprised of cylindrical cemented soil mass 200 mm in diameter with a steel tube reinforcement embedded in the center. The bond length between the steel tube and cemented soil was 80 mm. The steel tube reinforcement was 40 mm in outer diameter and 30 mm in inner diameter and was characterized by an elastic modulus of 210 GPa. The soil used in the cemented soil mix was prepared with moisture content of 65% and was mixed with cement with cement-to-soil mass ratio of 20%. Additional material properties for this test can be found in Chen et al. (2018, 2020). The pullout test was carried out on the element-scale specimen after a 28-day curing time using a customized pullout setup. Pullout load was applied to the reinforcement at a controlled displacement rate of 1 mm/min. The development of interface bond stress with the increasing pullout displacement was monitored and recorded during the loading process, as shown in Fig. 3.

The peak bond stress, residual bond stress, and initial shear stiffness were identified from the measured bond–slip curve. Subsequently, the interface characteristic parameters could be calibrated, where $\tau_f = 325$ kPa, $s_f = 1.1$ mm, $\tau_r = 156$ kPa, $k = \tau_r/\tau_f = 0.48$, and $k_{\text{ini}} = 465$ kPa·mm^{-1}. By substituting these interface characteristic parameters into Eq. (9), the values of bond–slip model parameters could be calculated, where $a = 372$, $b = 0.75$, $c = 156$, and $d = 1.18$. The prediction corresponding to the interface bond–slip model is presented in Fig. 3 along with the measured bond–slip curve. It was observed that the bond–slip model could effectively predict the bond–slip behavior in terms of both the prior-to-peak elastoplastic phase and the post-peak strain-softening phase.

The evolving contribution of adhesion and friction to interface bond strength over the increasing interface slip is illustrated in Fig. 4. The adhesion was observed to decrease rapidly after reaching the peak at interface slip of 1.1 mm, which indicated that the slip range to mobilize interface adhesion is comparatively small and the interface friction largely dominates the interface bond resistance at large slip ranges, particularly for the steel tube reinforcements in cemented soils.

Verification for the Developed Interface Model in Special Cases A and B

The availability of the developed integrated model has been examined using the element pullout testing results of steel tube embedded in cemented soils. The tested interface bond–slip response was conventional because the interface adhesion and interface friction existed together, as shown in Figs. 3 and 4.

Ma et al. (2013) studied the interface mechanical behavior between rock bolt and resin by laboratory pullout tests. The test results could be regarded as corresponding to the Special Case A (adhesion only) due to the inherent mechanical properties of the resin, and its interface bond–slip response ($L = 45$ mm) shown in

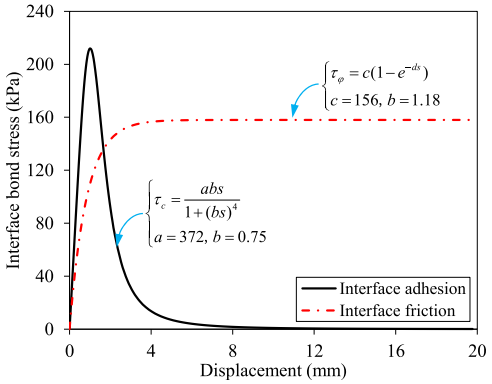

Fig. 4. Contributions of adhesion and friction in interface bond strength.

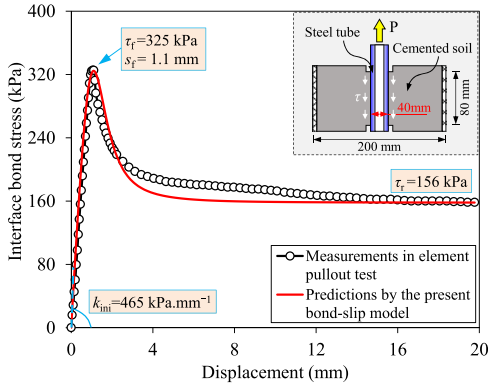

Fig. 3. Comparison between measurements and predictions of interface bond–slip response.

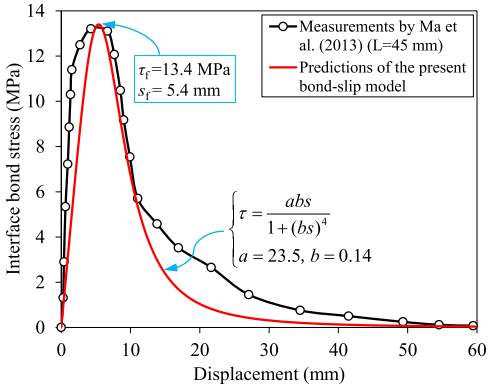

Fig. 5. Comparison between the predicted interface bond–slip response and the measurements tested by Ma et al. (2013).

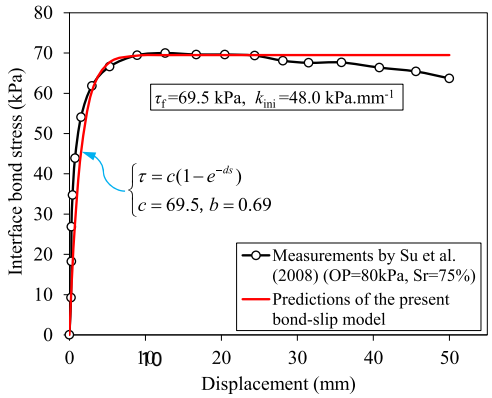

Fig. 6. Comparison between the predicted interface bond–slip response and the measurements tested by Su et al. (2008).

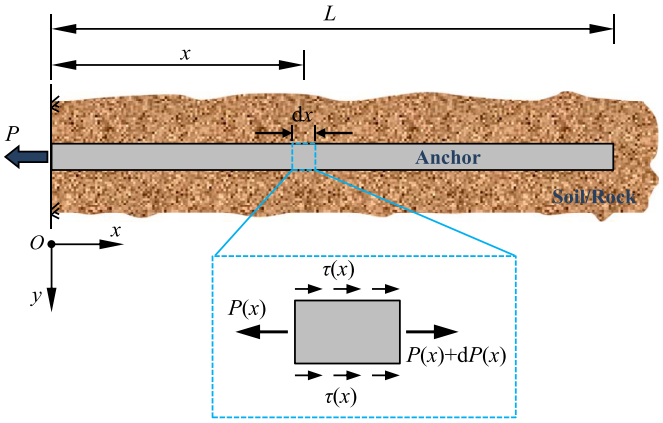

Fig. 7. Schematic of typical force analysis of anchor.

Fig. 5 also proved that. The present integrated model can thus be simplified as the form of Eq. (3) with only two parameters. The parameters of peak interface bond stress τ_f and its corresponding displacement s_f were 13.4 MPa and 5.4 mm, respectively. The model parameters could further be determined using Method B: $a = 23.5$, and $b = 0.14$.

Su et al. (2008) investigated the pullout resistance of soil nails embedded in completely decomposed granite (CDG). The CDG used can be classified as sandy soil because the content of gravel and sand reaches 71.84%, and its cohesion is almost zero in saturated condition. Hence, the tests can be regarded as corresponding to the Special Case B (friction only), and its interface bond–slip response (OP = 80 kPa, $S_r = 75\%$) shown in Fig. 6 also proved that. In this case, the present integrated model can thus be simplified as the form of Eq. (4) with only two parameters. The parameters of peak interface bond stress τ_f and initial shear stiffness k_{ini} were 69.5 kPa and 48.0 kPa·mm^{-1}, respectively. The model parameters could further be determined using Method B: $c = 69.5$, and $d = 0.69$.

As can be seen in Figs. 5 and 6, consistent agreements between the calculations and the two groups of test results validated adequately the versatility of the present interface bond–slip model.

Discussion for the Developed Interface Model

There are four parameters for the trilinear interface model (Benmokrane et al. 1995; Ren et al. 2010; Martin et al. 2011; Ma et al. 2016), three parameters for the hyperbolic model (Wong and Teh 1995) and parabolic model (Zhang et al. 2012), and two parameters for the exponential model (Liu et al. 2009) and dual exponential models (Ma et al. 2013; Huang et al. 2014). However, as mentioned, these bond–slip models are appropriate only to specific work conditions. The developed integrated model contains four parameters when the parameter n is determined based on the shape of the bond–slip curve (equal to 4 can be appropriate for most anchor cases). Conversely, the present model can be simplified, and its parameters are also reduced in some specific work conditions. For example, there are only two parameters in Special Cases A and B. Overall, the present integrated model provides a more robust adaptability in describing the soil–anchor interface behaviors, although it has more parameters than, for example, the hyperbolic model, parabolic model, and exponential model.

In addition, there are some factors that influence the interface mechanical behaviors of tensioned anchors/soil nails, including grouting pressure, overburden pressure, moisture content, soil types, and interface roughness. These factors have been studied adequately in previous works (e.g., Chu and Yin 2005; Su et al. 2008, 2010; Yin and Zhou 2009; Yin et al. 2009; Zhou et al. 2011; Chen et al. 2015, 2018, 2020; Ye et al. 2019), especially for the effects on interface shear strength. Note that the aforementioned factors can also affect the developed integrated bond–slip model by adjusting its form and the value of its parameters. For example, the soils around the anchors/soil nails are compacted with the increase of grouting pressure; the parameters a and c will increase because the interface shear strength increases almost linearly, and the parameters b and d will increase as well because the interface softening behavior becomes more significant (Yin and Zhou 2009; Yin et al. 2009; Zhou et al. 2011). With an increase of soil moisture content, the parameters a and c will decrease owing to the exponential decrease of soil–anchor interface shear strength, and the model form will gradually change from Eqs. (2) to (4) because the interface hardening behaviors become prominent (Zhang et al. 2020). The soil stresses around the anchors have been released during the drilling process of anchor hole (Su et al. 2008; Yin and Zhou 2009; Su et al. 2010). Hence, the impact induced by overburden pressure on soil–anchor interface bond behavior as well the developed integrated bond–slip model for the anchor in service was very limited in extent. Overall, it is recommended that engineers consider these factors carefully when determining model parameters.

Load-Transfer Modeling Framework

The integrated interface bond–slip model developed as part of this study was used in developing a load-transfer analytical framework for tensioned anchors. The implementation of this framework is described in this section. Fig. 7 shows the schematic for force analysis on a differential anchor element.

By applying static equilibrium of forces acting on the differential anchor element,

$$dP(x) + u_p \tau(x) dx = 0 \tag{13}$$

where $P(x)$ = axial force in the anchor at distance x; and u_p = cross-sectional perimeter of anchor.

The anchor can reasonably be assumed to be in elastic tension at working loads. Therefore,

$$ds = -\frac{P(x)}{EA} dx \tag{14}$$

where E = elastic modulus of the anchor; and A = cross-sectional area of the anchor. Assuming the tension rod and the grout deform

compatibly, the elastic modulus of the anchor can be calculated using composite stiffness, as

$$E = \frac{E_b A_b + E_g A_g}{A_b + A_g} \tag{15}$$

where E_b and E_g = elastic moduli of the tension rob and the grout, respectively; and A_b and A_g = cross-sectional areas of the tension rod and the grout, respectively. Combining Eqs. (13) and (14) derives

$$\frac{d^2 s(x)}{dx^2} - \frac{u_p \tau(x)}{EA} = 0 \tag{16}$$

The ratio of the cross-sectional perimeter to the axial stiffness of the anchor can be written as

$$\xi = \frac{u_p}{EA} \tag{17}$$

Substituting Eq. (2), Eq. (16) can be rewritten as

$$\frac{d^2 s(x)}{dx^2} - \xi\left[\frac{abs}{1 + (bs)^4} + c(1 - e^{-ds})\right] = 0 \tag{18}$$

The differential equation can be solved by separation of variables, as

$$p = \frac{ds(x)}{dx} = \varepsilon(x) \tag{19}$$

where $\varepsilon(x)$ = axial strain of the anchor,
and

$$\frac{d^2 s}{dx^2} = p\frac{dp}{ds} \tag{20}$$

By substituting Eq. (20) into Eq. (18) and integrating,

$$p = \sqrt{2\xi\left(\frac{a\ \mathrm{atan}(b^2 s^2)}{2b} + cs + \frac{ce^{-ds}}{d}\right) + C} \tag{21}$$

The boundary condition at the free end of the anchor can be expressed as

$$s(x = L) = s_L \tag{22a}$$

$$\varepsilon(x = L) = 0 \tag{22b}$$

By substituting Eq. (22) into Eq. (21),

$$C = -2\xi\left(\frac{a\ \mathrm{atan}(b^2 s_L^2)}{2b} + cs_L + \frac{ce^{-ds_L}}{d}\right) \tag{23}$$

By combining Eq. (23) and Eq. (21),

$$p = \sqrt{2\xi\left(\frac{a\mathrm{atan}(b^2 s^2)}{2b} + cs + \frac{ce^{-ds}}{d}\right) - 2\xi\left(\frac{a\mathrm{atan}(b^2 s_L^2)}{2b} + cs_L + \frac{ce^{-ds_L}}{d}\right)} \tag{24}$$

Based on Eq. (24), the displacement compatibility method (Seed and Reese 1957; Cao 1986) could be used to solve for the load-displacement response, as follows:

- Step 1: The bond length of the anchor is discretized into n segments uniformly by nodes numbered 0, 1, 2, …., $n-1$, n from loaded end to free end with the length of each segment of $\Delta L = L/n$. The value of n can be specified according to the computational precision demand.
- Step 2: The free end of anchor (i.e., node n) is assumed to have no axial displacement, that is, $s_L = 0$, and the loaded end of anchor (i.e., node 0) is prescribed with a pullout displacement s_0. The axial strain at loaded end of anchor $\varepsilon(0)$ can be calculated in Eq. (24).
- Step 3: Axial displacement at node 1 $s(1)$ can be calculated as $s_0 - \varepsilon(0)\Delta L$. Similarly, axial strain and axial displacement at the remaining nodes can be determined in sequence.
- Step 4: The calculated displacement at node n, $s(n)$, is used to update the value of s_L. Steps 2 through 3 are repeated until the value of $s(n)$ converges in subsequent iterations.
- Step 5: The converged displacement at the free end is substituted into Eq. (24), and the axial force and interface bond stress corresponding to each node can be determined using Eqs. (25) and (26), respectively:

$$P(i) = EA\varepsilon(i) \tag{25}$$

$$\tau(i) = \frac{abs(i)}{1 + (bs(i))^4} + c(1 - e^{-ds(i)}) \tag{26}$$

Hence, the distributions of the axial force and interface bond stress over the bond length can be solved for a given displacement at loaded end s_0. In particular, the axial force at the loaded end $P(0)$ (i.e., pullout force) can be determined as

$$P(0) = EA\varepsilon(0) = EA\sqrt{2\xi\left(\frac{a\ \mathrm{atan}(b^2 s_0^2)}{2b} + cs_0 + \frac{ce^{-ds_0}}{d}\right) - 2\xi\left(\frac{a\ \mathrm{atan}(b^2 s_L^2)}{2b} + cs_L + \frac{ce^{-ds_L}}{d}\right)} \tag{27}$$

- Step 6: Additional values of displacement at loaded end s_0 can be prescribed and Steps 2 through 5 can be repeated to solve for the anchor bond–slip response and for the distributions of axial force and interface bond stress over the anchor bond length.
- Step 7: The curve of pullout load versus pullout displacement at loaded end can be plotted.

Experimental Verification

The effectiveness and applicability of the presented integrated interface bond–slip model and load-transfer analysis framework can be examined in general by comparing the predicted and measured pullout response for different types of tensioned anchors. Pullout tests on steel tube in cemented soils, steel reinforcement in concrete, and glass fiber–reinforced polymer (GFRP) tendon in sand were typically carried out and/or used as representative case examples in this study to derive the measurements of anchor pullout response. These tests are described next.

Model Test of Tensioned Steel Tube Embedded in Cemented Soils

Cemented soils in soil mixing applications are often reinforced with steel bars, steel sections, or fiber reinforced polymer (FRP) materials

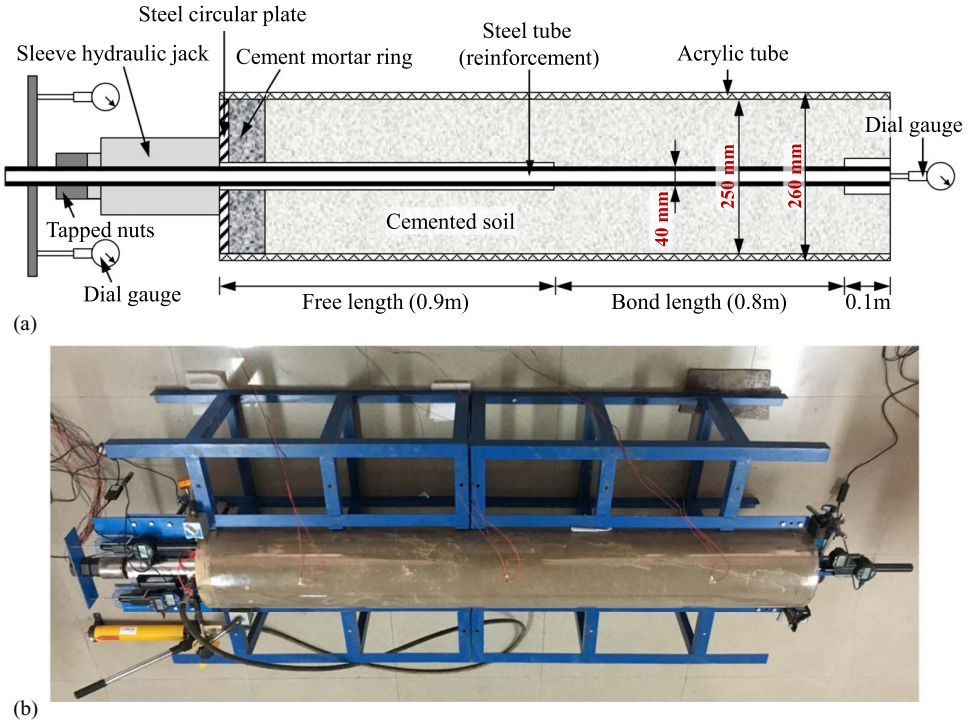

Fig. 8. Model test setup of steel tube reinforcement embedded in cemented soils: (a) schematical view; and (b) photographic view.

to improve the tensile resistance of the cemented soils (CECS 2016; Zhang 2018). A model test of reinforced soil mixing anchor subjected to pullout loads was carried out using cemented soil and reinforcement consistent with those used in element pullout test aiming to facilitate the verification between specimens in two different test scales. Specifically, the steel tube was 40 mm in outer diameter and 30 mm in inner diameter and was characterized by an elastic modulus of 210 GPa. The cemented soil prepared was 65% in moisture content, 20% in cement-to-soil mass ratio, and 3.33 MPa in unconfined compressive strength after curing 28 days. The setup, loading scheme, and results of the model test are discussed next.

Test Setup

The model specimen was prepared with a steel tube as reinforcement and cemented soils as a geomaterial where the reinforcement was embedded. As illustrated in Fig. 8(a), the model specimen was 250 mm in diameter, 0.8 m in bond length, 0.9 m in free length at loaded end, and 0.1 m in free length at free end. The influence zone of lateral friction resistance of a pile is generally between five to ten times that of the pile diameter (Cooke et al. 1979). Similar results were found for anchors via experimental investigation (Rajaie 1990; Chen et al. 2017). In the present model test, the ratio between the diameter of the specimen (250 mm) and the outer diameter of the steel tube reinforcement (40 mm) was 6.25, and the roughness of the steel tube–cemented soil interface is notably weaker than that of grouted anchors/piles. Hence, it can be inferred that the influence of scaling effect could almost be eliminated.

A self-balance loading technique was adopted in the present pullout model test (Rong et al. 2004; Zhang et al. 2015). Specifically, a sleeve hydraulic jack going through the steel tube reinforcement was installed with reaction on the free end of the model specimen. A circular steel plate and cement mortar ring were used under the base of the sleeve hydraulic jack to minimize stress concentration and transfer the reaction to the specimen. A relatively long free length (0.9 m) was designed to minimize the loading boundary effect and simulate the free segment of in situ tensioned

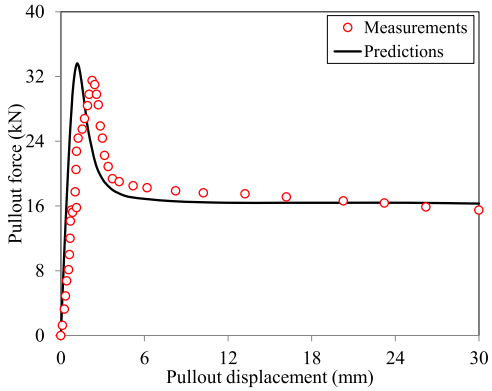

Fig. 9. Measured and predicted pullout load-displacement response for model test.

anchors. The internal surface of the acrylic tube was coated with petroleum jelly before pouring cemented soils to minimize boundary friction. This procedure is the same as that for preparing an element-scale pullout specimen, and its details could also be found in the publication of the previous work (Chen et al. 2018, 2020). The pullout load applied to the loaded end of reinforcement was monitored using a load cell, and the displacements of loaded and free ends of the reinforcement were recorded in real time using dial gauges. Details of the setup design are available in Zhang (2018). Figs. 8(a and b) depict a schematic and a photograph of the test setup, respectively.

Loading Scheme

A two-phase loading strategy (Yin and Zhou 2009) was used in applying pullout loads to the reinforcement: (1) prior-to-peak phase, where multistage loads were applied at each loading stage and the load was held for 30 min until reaching the peak pullout force; and (2) post-peak phase, where displacement-controlled loads were

applied after peak pullout load was observed by maintaining displacement rate of 0.6 mm/min.

Test Results

The load-displacement response measured in model test was compared with predictions derived using the load-transfer analytical framework on this model test, as shown in Fig. 9.

A good agreement between measurements and predictions for pullout resistance was observed. Specifically, the measured and predicted ultimate pullout resistance values were 31.5 and 33.6 kN, respectively, and the measured and predicted residual pullout resistance values were 15.5 and 16.3 kN, respectively. Overall, the predicted load-displacement curve shows a closer match with the measurements in the model test. It confirmed the applicability of Method B in calibrating the bond–slip model parameters and examined the effectiveness of the present load-transfer analytical framework.

Model Test of Tensioned Reinforcement Bar Embedded in Concrete

Rong et al. (2004) conducted a pullout test to investigate the working mechanism of tensioned anchors. The tension rod was modeled by a deformed reinforcement bar 32 mm in diameter and characterized by an elastic modulus of 210 GPa. The geomaterial was modeled by concrete $R_{28}200\#$ (i.e., 28-day curing compressive strength of 200 kg/mm^2). The reinforcement was fully encapsulated in concrete with 1.0 m bond length. Ten strain gauges were installed uniformly over the reinforcement surface to monitor the evolution of the axial force distribution as loading progressed.

Because it is not feasible to obtain interface characteristic parameters directly from the measurements of the test (Ma et al. 2016), the aforementioned Method A was used by some researchers (Ren et al. 2010; Martin et al. 2011; Ma et al. 2013, 2016; Huang et al. 2014) to interpret the measured pullout response and determine interface characteristic parameters corresponding to their interface bond–slip models, as illustrated in Fig. 10. Using the reported interface characteristic parameters, the values of model parameters of the integrated bond–slip model developed in this study could be determined, where $a = 10{,}900$ $b = 3.6$, $c = 420$, $d = 6.2$. Since the test data analyzed by these models are the same with that by the developed integrated model, they were selected for comparison as well in this paper. Fig. 10 shows predictions of interface bond–slip models reported in literature as well as the model developed in this study to characterize the interface behavior of the anchor in the model test.

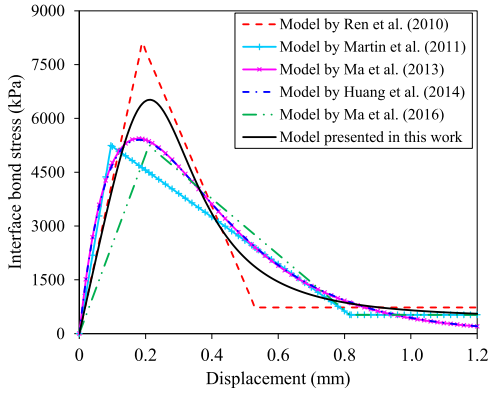

Fig. 10. Interface bond–slip models developed to characterize the interface behavior in the model test by Rong et al. (2004).

The load-transfer analysis of the anchor in the model test was performed using the integrated interface bond–slip model. Fig. 11 presents the pullout load-displacement curves predicted using the models summarized in Fig. 10 as well as that obtained experimentally (Rong et al. 2004). Predictions of the axial force and the interface bond stress distributions over the bond length of the anchor in the model test were compared with the measurements as shown in Figs. 12 and 13, respectively. As shown in these figures, the predictions developed using the integrated interface bond–slip model and the corresponding load-transfer analysis are in good agreement with the measured data. This agreement validates the effectiveness of the integrated interface bond–slip model and the load-transfer analytical framework developed in this study.

The anchor–soil interface manifests roughly complete strain-softening behavior in the pullout test conducted by Rong et al. (2004), with the reliable evidence shown in Fig. 10. It can be regarded as the Special Case A (adhesion only). However, for the Special Case B (friction only), these previous models, particularly for the dual exponential model (Ma et al. 2013; Huang et al. 2014), cannot be applicable due to the failure of characterizing the interface hardening behavior.

Pullout Test of GFRP Tendons Embedded in Sands

Zhang et al. (2015) investigated the pullout behavior of GFRP tendons of different diameters embedded in sands. A pullout test on a specimen with GFRP tendon of 5 mm in diameter, characterized by an elastic modulus of 20.4 GPa, and embedded in sand with 0.85 m

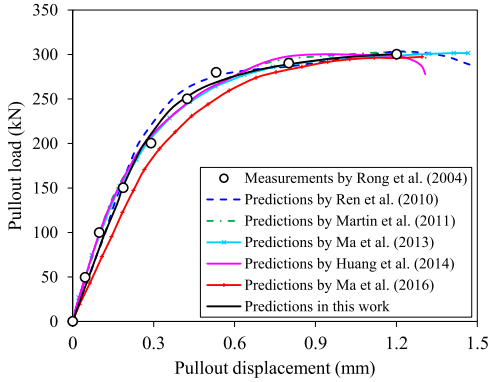

Fig. 11. Measurements and predictions of pullout load-displacement response of the anchor in the model test by Rong et al. (2004).

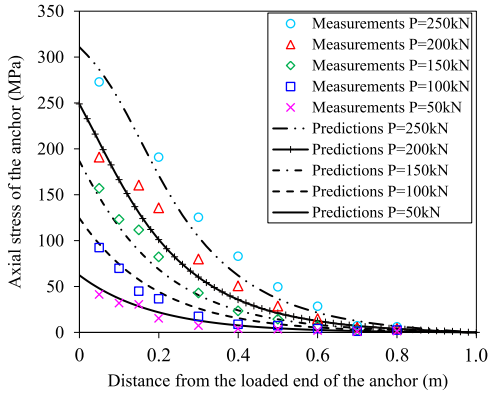

Fig. 12. Measured and predicted axial stress distribution over the bond length of the anchor under various pullout loads.

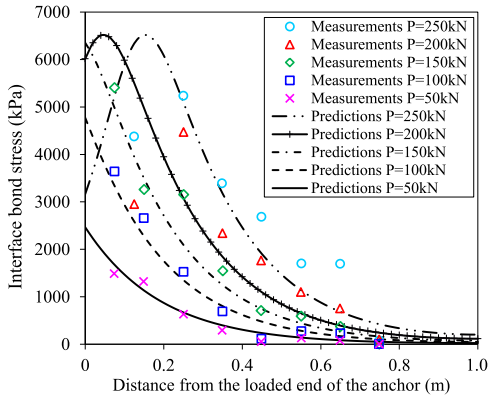

Fig. 13. Measured and predicted interface bond stress distribution over the bond length of the anchor under various pullout loads.

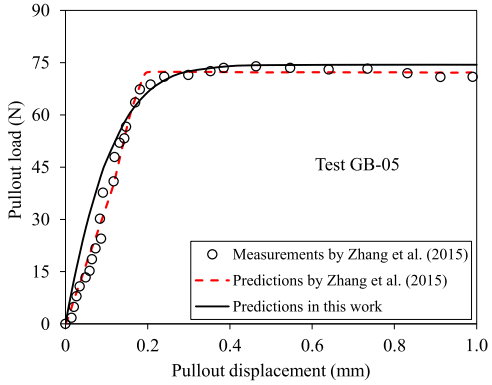

Fig. 14. Measurements and predictions of GFRP tendon embedded in sands.

bond length was used to validate the effectiveness of the load-transfer analytical framework developed in this study.

In this case, GFRP tendon–sand interface adhesion was assumed to be negligible due to the insignificant cohesion of sands. Special Case B was applied to establish interface bond–slip model for this case using Eq. (4). A bilinear interface bond–slip model was adopted in Zhang et al. (2015) to characterize the interface behavior with interface characteristic parameters $\tau_f =$ 8.51 kPa, $s_f = 0.12$ mm, $k = 1.0$, and secant shear stiffness $\bar{k} = \tau_f / s_f = 70.9$ kPa/mm. It should be noted that Zhang et al. (2015) determined the interface area as the projective area of GFRP tendon over the sand. By identifying the direct contact area of GFRP tendon in sands as the interface bond area, the interface characteristic parameters were updated as $\tau_f = 5.42$ kPa and $\bar{k} = 45.2$ kPa/mm. In addition, secant shear stiffness defined in slip ranging from 0 to s_f (0.12 mm) was transformed to initial shear stiffness $k_{\text{ini}} =$ 75.6 kPa/mm. Hence, the interface characteristic parameters of this case were determined as $\tau_f = 5.42$ kPa, $s_f = 0.12$ mm, $k = 1.0$, and $k_{\text{ini}} = 75.6$ kPa/mm. Substituting values of interface characteristic parameters into Eq. (12), the model parameters of interface bond–slip model in Eq. (4) can be determined as $c = 5.42$ and $d = 14.0$.

Pullout load-displacement response of GFRP tendon in this case example was obtained using the developed interface bond–slip model and corresponding a load-transfer analytical framework. Along with the measurements of the reported pullout test, Fig. 14 shows the pullout load-displacement responses predicted using the interface bond–slip model developed in this study and the bilinear interface bond–slip model (Zhang et al. 2015). It was observed that the predictions from the model developed in this study agree well with the reported measurements as well as the bilinear interface model predictions. This agreement validates the effectiveness of the developed interface bond–slip model in prediction of anchor behavior in Special Case B.

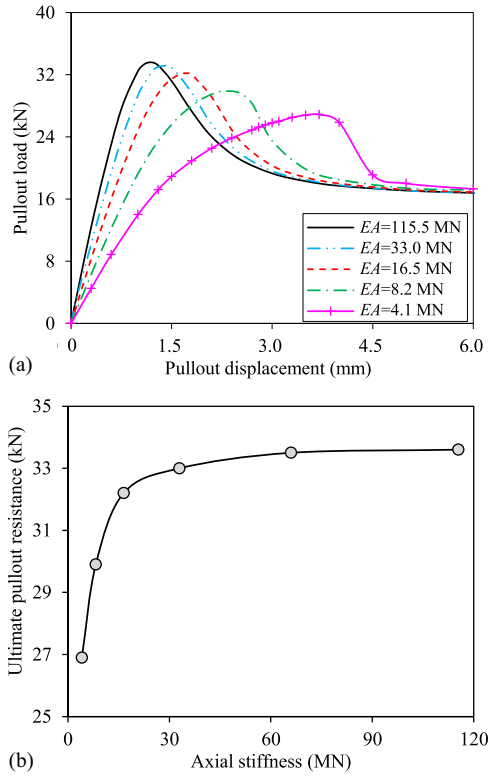

Fig. 15. Pullout response of anchors with various axial stiffnesses: (a) load-displacement responses; and (b) ultimate pullout resistance.

Parametric Study

The load-transfer analytical framework developed in this study was used to conduct parametric studies that investigated the impact of the effects of axial stiffness EA and bond length L on the pullout response. The configuration of the model test of tensioned steel tube embedded in cemented soils was used in the parametric studies.

Influence of Axial Stiffness on Pullout Response

Anchor–geomaterial stiffness is a key design aspect in attaining desired pullout resistances for anchors in the field. The axial stiffness of the reinforcement measured in model test was $EA = 115.5$ MN. The axial stiffness was varied over a range representative to axial stiffnesses of typical anchors, which were used with the load-transfer analytical framework to study the effect of the axial stiffness on the pullout response. Figs. 15(a and b) presents the pullout load-displacement response and ultimate pullout resistance of anchors with various axial stiffnesses, respectively. It was observed that the ultimate pullout resistance decreases with decreasing EA. In addition, the displacement at which ultimate pullout resistance is mobilized increases with decreasing EA. This signifies that anchors with comparatively lower axial stiffnesses tend to exhibit more ductile failure compared with those with comparatively higher axial stiffness. It was also observed from Fig. 15(b) that

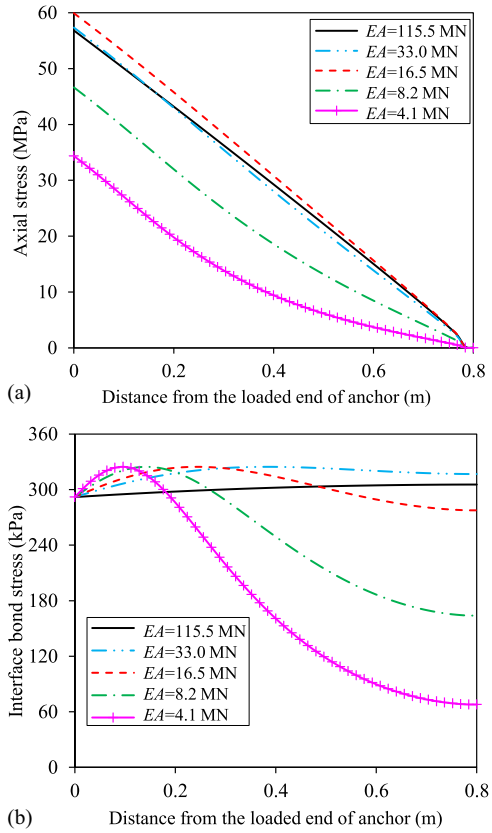

Fig. 16. Load-transfer response of anchors with various axial stiffnesses: (a) axial force distribution; and (b) interface bond stress distribution.

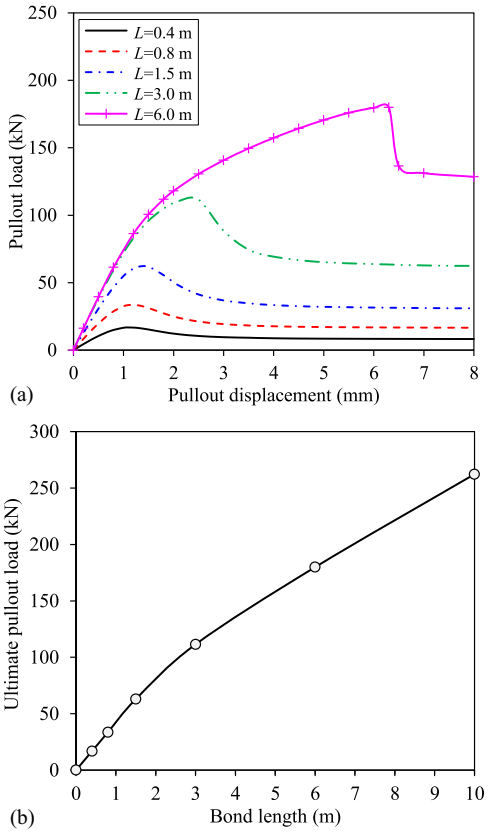

Fig. 17. Pullout response of anchors with various bond lengths: (a) load-displacement responses; and (b) ultimate pullout resistances.

ultimate pullout resistance is practically insensitive to the anchor's axial stiffness at relatively high stiffness values. Hence, it is recommended in design practice to avoid anchors with overly high stiffness provided the pullout resistance can be achieved.

Influence of Axial Stiffness on Load-Transfer Response

Distributions of axial force and interface bond stress over the anchor's bond length are usually used to evaluate the mobilization extent of anchor pullout resistance at different displacement conditions. Anchors with interface bond strength uniformly mobilized over the bond length are preferred in design. Variations of axial force and bond stress distribution over the same bond length at constant pullout displacement ($s = 1.5$ mm) were assessed for various anchor axial stiffness, as shown in Figs. 16(a and b), respectively.

The axial force distribution transforms from linear to nonlinear with decreasing EA. In particular, the axial force at the loaded end (i.e., pullout load) at $s = 1.5$ mm tends to increase within increasing EA. Like ultimate pullout resistance [Fig. 15(b)], this trend is pronounced only for anchors with comparatively small axial stiffnesses. This indicates that the compatibility of anchor–geomaterial interface stiffness and anchor axial stiffness should be considered in assessing pullout resistances of anchors.

With the decreasing axial stiffness, the interface bond stress changes from an approximately uniform distribution to a highly nonuniform distribution with bond stress hump near the loaded end. This hump was more pronounced and was observed closer to the loading end in anchors with lower axial stiffnesses. The distribution change can be explained as follows. (a) Anchors with comparatively large axial stiffnesses experience small axial strain, and thus the displacement of the free end (s_L) is like that of the loaded end. When the displacement at the free end is greater than the displacement corresponding to the peak bond stress of the bond–slip model (s_f), the interface is entirely at strain-softening stress condition. (b) The elastic deformation increases with decreasing axial stiffness, which leads to the less displacements at free end compared with the loading end. When $s_L = s_f$, the peak bond stress occurs at the free end and the entire bond length is still at strain-softening stress condition. (c) When s_L is smaller than s_f with decreasing axial stiffness, the elastic and strain-softening stress conditions (pre-peak and post-peak) occurs simultaneously over bond length, and the switch point of stress condition is characterized by the occurrence of peak bond stress, as exemplified by distributions of $EA = 16.5$, 8.2 and 4.1 MN in Fig. 16(b). (d) The decreasing axial stiffness results in increasing active bond length with elastic stress condition (pre-peak) and decreasing bond part with strain-softening stress condition (post-peak), and the point with peak bond stress shifts toward the loaded end.

Influence of Bond Length on Pullout Response

The interface bond stress is commonly assumed to uniformly distribute over bond length in current practice for anchors embedded in homogenous soils. This assumption leaves the bond length as the primary design variable to attain the desired pullout resistances. However, the interface bond stress tends to develop in highly nonlinear distributions over bond lengths. Assuming a linear relationship between bond length and pullout resistance should be improved by considering the nonlinearity of bond

stress distribution. This parametric study involved varying bond length from 0.4 to 6.0 m in the load-transfer analysis to study its effect on the pullout response and pullout resistance, as shown in Fig. 17.

The pullout load-displacement response varies substantially with varying bond length, as shown in Fig. 17(a). In particular, the displacement at which ultimate pullout resistance develops increases with increasing bond length. In addition, the rate of decrease in post-peak pullout resistance with increasing displacement was observed to increase with increasing bond length, which indicates decrease in failure ductility. Fig. 17(b) shows the relationship between the ultimate pullout resistance and bond length. It was observed that the relationship is nonlinear where the effect of changing the bond length on the ultimate pullout resistance decreases with increasing bond length.

Conclusions

A generalized load-transfer modeling framework for tensioned anchor was implemented in this study by developing a versatile interface bond–slip model based on adhesion–cohesion integration. Element-scale and large-scale model tests of a steel tube embedded in cemented soils were carried out as part of this study. The experimental data of these tests along with additional data from literature were used to validate the applicability and effectiveness of the developed interface bond–slip model and the load-transfer modeling framework. Finally, a parametric study was conducted. The key conclusions drawn from this study can be summarized as follows:

- The integrated interface bond–slip model developed in this study is applicable with versatility to characterize interface bond behavior of tensioned anchors embedded in different geomaterials, in particular modeling the full-range interface behavior.
- Laboratory pullout tests on element-scale anchor specimens were found effective in determining model parameters of interface bond–slip models. The accuracy of determined model parameters was found to depend on the consistency of testing conditions of specimens in element-scale with those of anchors conditions in situ.
- The generalized load-transfer modeling framework based on the presented interface bond–slip model could predict the pullout load-displacement response and the interface bond stress mobilization over the bond length with large scales representative to field scales for different types of tensioned anchors.
- It is recommended to design axial stiffness and bond length of anchor considering stiffness compatibility with anchor–geomaterial interfaces.

Overall, this work presented a generalized interface bond–slip model suitable for practitioners to use in design of tensioned anchors. The findings of this work provide insights into interface bond mobilization and pullout resistance development for tensioned anchors.

Data Availability Statement

All data, models, and code generated or used during the study appear in the published article.

Acknowledgments

This research was sponsored by the National Natural Science Foundation of China (Grant Nos. 41572298, 51978254 and 51908201), Natural Science Foundation of Hunan Province (Grant No. 2020JJ5024), and Hunan Provincial Innovation Foundation for Postgraduate (Grant No. CX20210410). The authors appreciate their support.

References

ACI (American Concrete Institute). 2003. *Bond and development of straight reinforcing bars in tension*. ACI 408R-03. Farmington Hills, MI: ACI.

Benmokrane, B., A. Chennouf, and H. S. Mitri. 1995. "Laboratory evaluation of cement-based grouts and grouted rock anchors." *Int. J. Rock Mech. Min. Sci.* 32 (7): 633–642. https://doi.org/10.1016/0148-9062(95)00021-8.

Cai, Y., T. Esaki, and Y. J. Jiang. 2004. "An analytical model to predict axial load in grouted rock bolt for soft rock tunneling." *Tunnelling Underground Space Technol.* 19: 607–618. https://doi.org/10.1016/j.tust.2004.02.129.

Cao, H. Z. 1986. "Axial loading transfer of pile and numerical calculation method of loading-settlement curve." *Chin. J. Geotech. Eng.* 8 (6): 37–49.

CECS (China Association for Engineering Construction Standardization). 2005. *Technical specification for ground anchors*. CECS 22. Beijing: China Planning Press.

CECS (China Association for Engineering Construction Standardization). 2016. *Technical specification for soil mass with reinforced cement soil pile and anchors*. CECS 147. Beijing: China Planning Press.

CEN (European Committee for Standardization). 2013. *Execution of special geotechnical works – Ground anchors*. EN 1537. Brussels, Belgium: CEN.

Chen, C. F., G. T. Liang, Y. Tang, and Y. L. Xu. 2015. "Anchoring solid-soil interface behavior using a novel laboratory testing technique." *Chin. J. Geotech. Eng.* 37 (6): 1115–1122.

Chen, C. F., G. B. Zhang, J. G. Zornberg, A. M. Morsy, and J. B. Huang. 2020. "Interface bond behavior of tensioned glass fiber-reinforced polymer (GFRP) tendons embedded in cemented soils." *Constr. Build. Mater.* 263: 120132. https://doi.org/10.1016/j.conbuildmat.2020.120132.

Chen, C. F., G. B. Zhang, J. G. Zornberg, A. M. Morsy, S. M. Zhu, and H. B. Zhao. 2018. "Interface behavior of tensioned bars embedded in cement-soil mixtures." *Constr. Build. Mater.* 186: 840–853. https://doi.org/10.1016/j.conbuildmat.2018.07.211.

Chen, J. H., P. C. Hagan, and S. Saydam. 2017. "Sample diameter effect on bonding capacity of fully grouted cable bolts." *Tunnelling Underground Space Technol.* 68: 238–243. https://doi.org/http://dx.doi.org/10.1016/j.tust.2017.06.004.

Chen, L. Z., G. Q. Liang, J. Y. Zhu, and W. Ge. 1994. "Analytical calculation of axial loading-settlement curve of piles." *Chin. J. Geotech. Eng.* 16 (6): 30–38.

Chu, L. M., and J. H. Yin. 2005. "Comparison of interface shear strength of soil nails measured by both direct shear box tests and pullout tests." *J. Geotech. Geoenviron. Eng.* 131: 1097–1107. https://doi.org/10.1061/(ASCE)1090-0241(2005)131:9(1097).

Cooke, R. W., G. Price, and K. Tarr. 1979. "Jacked piles in London clay: A study of load transfer and settlement under working conditions." *Géotechnique* 29 (2): 113–147. https://doi.org/10.1680/geot.1979.29.2.113.

Farmer, I. W. 1975. "Stress distribution along a resin grouted rock anchor." *Int. J. Rock Mech. Min. Sci.* 12: 347–351. https://doi.org/10.1016/0148-9062(75)90168-0.

GB (Guobiao Standard). 2013. *Technical code for building slope engineering*. GB 50330. Beijing: China Architecture & Building Press.

Heydinger, A. G., and M. W. O'Neill. 1986. "Analysis of axial pile-soil interaction in clay." *Int. J. Numer. Anal. Methods Geomech.* 10: 367–381. https://doi.org/10.1002/nag.1610100403.

Hong, C. Y., J. H. Yin, W. H. Zhou, and H. F. Pei. 2012. "Analytical study on progressive pullout behavior of a soil nail." *J. Geotech. Geoenviron. Eng.* 138: 500–507. https://doi.org/10.1061/(ASCE)GT.1943-5606.0000610.

Huang, M. H., Z. Zhou, and J. P. Ou. 2014. "Nonlinear full-range analysis of load transfer in fixed segment of tensile anchors." *Chin. J. Rock Mech. Eng.* 33 (11): 2190–2199.

Hu, L. M., and J. L. Pu. 2004. "Testing and modeling of soil-structure interface." *J. Geotech. Geoenviron. Eng.* 130 (8): 851–860. https://doi.org/10.1061/(ASCE)1090-0241(2004)130:8(851).

Hyett, A. J., M. Moosavi, and W. F. Bawden. 1996. "Load distribution along fully grouted bolts, with emphasis on cable bolt reinforcement." *Int. J. Numer. Anal. Methods Geomech.* 20 (7): 517–544. https://doi.org/10.1002/(SICI)1096-9853(199607)20:7<517::AID-NAG833>3.0.CO;2-L.

Kezdi, A. 1957. "Bearing capacity of piles and pile groups." In Vol. 2 of *Proc., of the 4th Int. Conf. on Soil Mechanics and Foundation Engineering*, 46–51. London: Butterworths.

Kılıc, A., E. Yasar, and A. G. Celik. 2002. "Effect of grout properties on the pull-out load capacity of fully grouted rock bolt." *Tunnelling Underground Space Technol.* 17: 355–365. https://doi.org/10.1016/S0886-7798(02)00038-X.

Kishida, H., and M. Uesugi. 1987. "Tests of the interface between sand and steel in the simple shear apparatus." *Geotechnique* 37 (1): 45–52. https://doi.org/10.1680/geot.1987.37.1.45.

Kraft, L. M., R. P. Ray, and T. Kagawa. 1981. "Theoretical t-z curves." *J. Geotech. Eng. Div.* 107 (11): 1543–1561. https://doi.org/10.1061/AJGEB6.0001207.

Li, C., and B. Stillborg. 1999. "Analytical models for rock bolts." *Int. J. Rock Mech. Min. Sci.* 36 (8): 1013–1029. https://doi.org/10.1016/S1365-1609(99)00064-7.

Liu, C. N., J. G. Zornberg, T. C. Chen, Y. H. Ho, and B. H. Lin. 2009. "Behavior of geogrid-sand interface in direct shear mode." *J. Geotech. Geoenviron. Eng.* 135 (12): 1863–1871. https://doi.org/10.1061/(ASCE)GT.1943-5606.0000150.

Martinez, A., J. D. Frost, and G. L. Hebeler. 2015. "Experimental study of shear zones formed at sand/steel interfaces in axial and torsional axisymmetric tests." *Geotech. Test. J.* 38 (4): 20140266. https://doi.org/10.1520/GTJ20140266.

Martín, L. B., M. Tijani, and F. Hadj-Hassen. 2011. "A new analytical solution to the mechanical behaviour of fully grouted rockbolts subjected to pull-out tests." *Constr. Build. Mater.* 25 (2): 749–755. https://doi.org/10.1016/j.conbuildmat.2010.07.011.

Ma, S. Q., J. Nemcik, and N. Aziz. 2013. "An analytical model of fully grouted rock bolts subjected to tensile load." *Constr. Build. Mater.* 49: 519–526. https://doi.org/10.1016/j.conbuildmat.2013.08.084.

Ma, S. Q., Z. Y. Zhao, W. Nie, and Y. L. Gui. 2016. "A numerical model of fully grouted bolts considering the tri-linear shear bond–slip model." *Tunnelling Underground Space Technol.* 54: 73–80. https://doi.org/10.1016/j.tust.2016.01.033.

Moayed, R. Z., M. Hosseinali, S. M. Shirkhorshidi, and J. Sheibani. 2019. "Experimental investigation and constitutive modeling of grout–sand interface." *Int. J. Geomech.* 19 (5): 04019024. https://doi.org/10.1061/(ASCE)GM.1943-5622.0001384.

PTI (Post-Tensioning Institute). 2014. *Recommendations for prestressed rock and soil anchors*. 5th ed. DC35.1-14. Phoenix, AZ: PTI.

Rajaie, H. 1990. "Experimental and numerical investigations of cable bolt support systems." Ph.D. thesis. Dept. of Mining and Metallurgical Engineering, McGill Univ.

Ren, F. F., Z. J. Yang, J. F. Chen, and W. W. Chen. 2010. "An analytical analysis of the full-range behaviour of grouted rockbolts based on a tri-linear bond-slip model." *Constr. Build. Mater.* 24: 361–370. https://doi.org/10.1016/j.conbuildmat.2009.08.021.

Richard, R. M., and B. J. Abbott. 1975. "Versatile elastic-plastic stress-strain formula." *J. Eng. Mech. Div.* 101 (4): 511–515. https://doi.org/10.1061/JMCEA3.0002047.

Rong, G., H. C. Zhu, and C. B. Zhou. 2004. "Testing study on working mechanism of fully grouted bolts of thread steel and smooth steel." *Chin. J. Rock Mech. Eng.* 23 (3): 469–475.

Satoru, S. 1965. "Mechanism of bearing capacity of the pile." *Civ. Eng. Technol.* 20 (1): 1–5.

Seed, H. B., and L. C. Reese. 1957. "The action of soft clay along friction piles." *Trans. Am. Soc. Civ. Eng.* 122 (1): 731–754. https://doi.org/10.1061/TACEAT.0007501.

Su, L. J., T. C. F. Chan, J. H. Yin, Y. K. Shiu, and S. L. Chiu. 2008. "Influence of overburden pressure on soil–nail pullout resistance in a compacted fill." *J. Geotech. Geoenviron. Eng.* 134: 1339–1347. https://doi.org/10.1061/(ASCE)1090-0241(2008)134:9(1339).

Su, L. J., J. H. Yin, and W. H. Zhou. 2010. "Influences of overburden pressure and soil dilation on soil nail pull-out resistance." *Comput. Geotech.* 37: 555–564. https://doi.org/10.1016/j.compgeo.2010.03.004.

Toufigh, V., S. M. Shirkhorshidi, and M. Hosseinali. 2017. "Experimental investigation and constitutive modeling of polymer concrete and sand interface." *Int. J. Geomech.* 17 (1): 04016043. https://doi.org/10.1061/(ASCE)GM.1943-5622.0000695.

Vijayvergiya, V. N. 1977. "Load-movement characteristics of piles." In *Proc., 4th Annual Symp. of the Waterway, Port, Coastal, and Ocean Division of ASCE*, 269–284. New York: ASCE.

Wang, M. 1983. "Mechanism of full-column rock bolt." *J. China Coal Soc.* 1: 40–47.

Wong, K. S., and C. I. Teh. 1995. "Negative skin friction on piles in layered deposits." *J. Geotech. Eng.* 121 (6): 457–465. https://doi.org/10.1061/(ASCE)0733-9410(1995)121:6(457).

Ye, X. Y., Q. Wang, S. Y. Wang, S. Sloan, and D. C. Sheng. 2019. "Performance of a compaction-grouted soil nail in laboratory tests." *Acta Geotech.* 14: 1049–1063. https://doi.org/10.1007/s11440-018-0693-y.

Yin, J. H., L. J. Su, R. W. M. Cheung, Y. K. Shiu, and C. Tang. 2009. "The influence of grouting pressure on the pullout resistance of soil nails in compacted completely decomposed granite fill." *Geotechnique* 59 (2): 103–113. https://doi.org/10.1680/geot.2008.3672.

Yin, J. H., and W. H. Zhou. 2009. "Influence of grouting pressure and overburden stress on the interface resistance of a soil nail." *J. Geotech. Geoenviron. Eng.* 135: 1198–1208. https://doi.org/10.1061/(ASCE)GT.1943-5606.0000045.

You, C. A. 2000. "Mechanical analysis on wholly grouted anchor." *Chin. J. Rock Mech. Eng.* 19 (3): 339–341.

You, C.A. 2004. "Theory and application study on stress-transfer mechanism of anchoring system." Ph.D. thesis, College of Natural Resources and Environmental Engineering, Shandong Univ. of Science and Technology.

Yu, C., and S. Y. Liu. 2005. "Research on behaviors of single pile considering softening of pile-side soil." *Rock Soil Mech.* 26 (S1): 133–136.

Zhang, C. C., H. H. Zhu, B. Shi, F. D. Wu, and J. H. Yin. 2015. "Experimental investigation of pullout behavior of fiber-reinforced polymer reinforcements in sand." *J. Compos. Constr.* 19 (3): 04014062. https://doi.org/10.1061/(ASCE)CC.1943-5614.0000526.

Zhang, G. B., C. F. Chen, J. G. Zornberg, A. M. Morsy, and F. S. Mao. 2020. "Interface creep behavior of grouted anchors in clayey soils: Effect of soil moisture condition." *Acta Geotech.* 15: 2159–2177. https://doi.org/10.1007/s11440-019-00907-6.

Zhang, G.B. 2018. "Interface characterization and load transfer analyses for anchored systems." Ph.D. thesis. College of Civil Engineering, Hunan Univ.

Zhang, Q. Q., and Z. M. Zhang. 2012. "A simplified nonlinear approach for single pile settlement analysis." *Can. Geotech. J.* 49 (11): 1256–1266. https://doi.org/10.1139/t11-110.

Zhou, W. H., J. H. Yin, and C. Y. Hong. 2011. "Finite element modeling of pullout testing on a soil nail in a pullout box under different overburden and grouting pressures." *Can. Geotech. J.* 48: 557–567. https://doi.org/10.1139/t10-086.

Zhu, H., and M. F. Chang. 2002. "Load transfer curves along bored piles considering modulus degradation." *J. Geotech. Geoenviron. Eng.* 128 (9): 764–774. https://doi.org/10.1061/(ASCE)1090-0241(2002)128:9(764).

Zhu, S. M., C. F. Chen, F. S. Mao, and H. Cai. 2021. "Application of disturbed state concept for load-transfer modeling of recoverable anchors in layer soils." *Comput. Geotech.* 137: 104292. https://doi.org/10.1016/j.compgeo.2021.104292.

Zou, J. F., and P. H. Zhang. 2019. "Analytical model of fully grouted bolts in pull-out tests and in situ rock masses." *Int. J. Rock Mech. Min. Sci.* 113: 278–294. https://doi.org/10.1016/j.ijrmms.2018.11.015.